Optical Forces in Plasmonic Nanoparticle Dimers†

ARTICLE *in* THE JOURNAL OF PHYSICAL CHEMISTRY C · APRIL 2010

Impact Factor: 4.77 · DOI: 10.1021/jp911371r

Optical Forces in Plasmonic Nanoparticle Dimers[†]

Vladimir D. Miljković,[‡] Tavakol Pakizeh,[‡,§] Borja Sepulveda,[∥] Peter Johansson,[‡,⊥] and Mikael Käll*[,‡]

Department of Applied Physics, Chalmers University of Technology, S-412 96 Göteborg, Sweden, Department of Electrical Engineering, K.N. Toosi University of Technology, 16314 Tehran, Iran, Nanobiosensors and Molecular Nanobiophysics Group, Research Centre in Nanoscience and Nanotechnology (CIN2) CSIC-ICN, 08193 Bellaterra, Barcelona, Spain, and School of Science and Technology, Örebro University, S-701 82 Örebro, Sweden

Received: November 30, 2009; Revised Manuscript Received: January 26, 2010

We present calculations of the optical forces between two metal nanospheres forming a hybridized plasmonic dimer. We consider homo- and heterodimers and investigate different plane wave illumination configurations. The forces between the particles are calculated using full Mie theory combined with the Maxwell stress tensor (MST) formalism, as well as by approximate methods, such as the Lorentz force (LF) approach taken in the dipole limit and calculations based on an optical potential. We show that the simplified calculation schemes can lead to serious errors in the case of strongly interacting particles and low damping. In particular, we find that equilibrium configurations, corresponding to vanishing optical forces, only are possible for homodimers illuminated in the end-fire configuration and for heterodimers, although multipolar effects and damping radically reduce the repulsive interactions in the latter case.

1. Introduction

As first proposed by Martin Moskovits in 1978,[1] surface-enhanced Raman scattering (SERS) originates from an electromagnetic (EM) field enhancement generated by localized surface plasmon resonances (LSPRs).[2] SERS is, however, not the only application enabled by plasmonic field enhancement. For example, light emission from tunnel junctions[3] and scanning tunneling microscopes (STM)[4] also rely on a field enhancement effect brought about by plasmons. The rapid development of nanotechnology and EM simulation capacity over the past decade has resulted in the development of a vast range of novel nanoplasmonic applications, many of which essentially build on the discovery of SERS.[5–7] Examples include LSPR refractive index sensing,[8,9] photodynamic therapy,[10] nanoscopic antennas,[11,12] and metamaterials.[13] One area of increasing interest is to utilize plasmonic field enhancement to amplify optical forces.

Optical forces are well-known from the field of laser tweezers, developed by Ashkin and co-workers in the 80s as a method to trap and manipulate microscopic dielectric objects using a tightly focused laser beam.[14] The technique is based on the so-called gradient force, which in the small particle limit can be rationalized in terms of an optical potential $U = -\langle \mathbf{p}\cdot\mathbf{E}\rangle$. Here, $\mathbf{p} = \alpha\mathbf{E}$ is the dipole moment induced in the particle by the spatially varying laser field $\mathbf{E}(\mathbf{r})$, leading to a force $\mathbf{F}(\mathbf{r}) = \alpha\nabla E^2(\mathbf{r})$ directed toward the point of highest intensity and with strength proportional to the particle polarizability α. Classical single beam laser tweezers based on the gradient force can be used to manipulate also metal nanoparticles supporting LSPRs, as recently demonstrated by trapping of silver[15] and gold colloids.[16] It has even been shown that polarization dependent gradient forces and torques can be used to rotate and spin elongated nanoplasmonic systems, including nanoparticle dimers.[17] However, field enhancement and localization associated with LSPR can also be utilized to dramatically increase the strength and spatial resolution of the gradient force acting on small dielectric objects. This concept was first investigated for the case of sharp metal tips[18–20] and recently exploited using lithographically prepared nanoplasmonic surfaces.[21–25] In this contribution, however, we discuss LSPR enhanced optical forces between nanoparticles. We focus on the prototypical near-field coupled nanoplasmonic system well-known from the SERS field,[26–29] i.e., two interacting metal nanospheres forming a dimer. The optical forces induced by and acting on such a dimer were studied theoretically by Xu and Käll, who found a substantial plasmon enhanced attractive force at short surface-to-surface separations.[30] This result was also corroborated by extended EM simulations studies by several groups,[31–42] as well as by SERS experiments on optically aggregated silver colloids.[43–45] Here we revisit the dimer system with the objective of clarifying some remaining issues, in particular concerning the accuracy and implementation of the dipole approximation in the context of forces between coupled particles and the question whether optical forces can lead to an equilibrium distance between interacting nanoparticles.[46]

2. Methods

2.1. Maxwell Stress Tensor and Mie theory (MST−Mie). In Mie theory, a monochromatic electric field just outside a spherical particle can be written[29]

[†] Part of the "Martin Moskovits Festschrift".

* To whom correspondence should be addressed. E-mail: kall@chalmers.se.

[‡] Chalmers University of Technology.

[§] K.N. Toosi University of Technology.

[∥] CSIC-ICN.

[⊥] Örebro University.

10.1021/jp911371r
Published on Web 02/17/2010

$$\boldsymbol{E} = \sum_{lm} [a_{1lm} j_l(kr) + b_{1lm} h_l(kr)]\mathbf{X}_{lm} + k^{-1}\nabla \times \{[a_{2lm} j_l(kr) + b_{2lm} h_l(kr)]\mathbf{X}_{lm}\} \quad (1)$$

The first term, with a_{1lm} and b_{1lm}, is the magnetic multipole contribution and the second term is the electric multipole contribution. The terms involving the spherical Bessel functions j_l describe regular (i.e., nonsingular at $r = 0$), incident waves, and the terms with spherical Hankel functions, h_l, scattered, outgoing waves. $\mathbf{X}_{lm}$ denotes the vector spherical harmonics and $k = n\omega/c$ the wave vector, with n defining the refractive index of the material surrounding the particle. The strengths of the outgoing scattered waves are related to those of the incident waves through sphere response functions $s_l^{M(E)} = b_{1(2)lm}/a_{1(2)lm}$. The incident wave coefficients depend on, and can be determined from, the strength of the incoming plane wave and the magnitude of the waves scattered from the other particle or particles in the interacting system.[29] In the case of a particle that only responds as an electric dipole, the only outgoing waves that occur are the ones described by the coefficients b_{21m} with $m = 0, \pm 1$. These coefficients are directly related to the induced dipole moments p_x, p_y, and p_z.

We calculate the optical force acting on a given particle by integrating the Maxwell stress tensor over a surface surrounding that particular particle. We have

$$F_\alpha = \int_S T_{\alpha\beta} n_\beta \, \mathrm{d}S \quad (2)$$

where n_β denotes a component of a normal vector $\hat{n}$ to the integration surface, and the Maxwell stress tensor is given by

$$T_{\alpha\beta} = \frac{1}{4\pi}\left[\varepsilon E_\alpha E_\beta + B_\alpha B_\beta - \frac{1}{2}(\varepsilon \mathbf{E}\cdot\mathbf{E} + \mathbf{B}\cdot\mathbf{B})\delta_{\alpha\beta}\right] \quad (3)$$

When the field is expressed in terms of vector spherical harmonics, the force can be calculated analytically; that is, eq 2 does not have to be evaluated through direct numerical integration. This is most easily done by employing methods from quantum mechanics designed to deal with spherical symmetry, such as the Wigner−Eckhardt theorem.[47] For the z component of the force, this leads to

$$\langle F_z \rangle = \frac{\varepsilon}{8\pi k^2}\left[\sum_{\tau=1}^{2}\sum_{l=1}^{l_{\max}}\sum_{m=-l}^{l} \mathrm{Im}\{a^*_{\tau l+1,m} b_{\tau lm} + b^*_{\tau l+1,m} a_{\tau lm} + 2b^*_{\tau l+1,m} b_{\tau lm}\}\frac{\sqrt{l(l+2)}}{l+1}\sqrt{\frac{(l+m+1)(l-m+1)}{(2l+1)(2l+3)}} - \sum_{l=1}^{l_{\max}}\sum_{m=-l}^{l} \mathrm{Re}\{a^*_{1lm} b_{2lm} + b^*_{1lm} a_{2lm} + 2b^*_{1lm} b_{2lm}\}\frac{m}{l(l+1)}\right] \quad (4)$$

There are similar expressions for the x and y components of the force, see for example the work of Barton et al.[48] Although expression 4 looks rather formidable, it still reveals an underlying, fairly simple, structure. The force originates from products of multipoles of the same type with l differing by 1, or from products of different multipoles with the same l.

In the important approximation of a particle only responding as an electric dipole, only two of the six terms in eq 4 contribute to the force: the first term on the left-hand side corresponds to the force on the dipole proportional to the gradient of the incident electric field and the first term after the minus sign describes the force that the incident magnetic field causes.

Mie theory together with the Maxwell stress tensor formalism gives us a rigorous scheme for calculating the optical force between spherical particles to any given level of accuracy, as determined by the total number of multipoles included in the calculation. Nevertheless, it is an advantage to have alternative methods that are simpler to handle in various contexts. Next we look at a number of such alternatives.

2.2. Maxwell Stress Tensor and the Coupled Dipole Approximation (MST−CDA). The optical response of a collection of interacting nanoparticles can be estimated from the CDA method,[49,50] which is based on solving a system of coupled dipole equations

$$\mathbf{p}_i = \alpha_i \mathbf{E}_i = \alpha_i(\mathbf{E}_{\mathrm{inc},i} - \sum_{j\neq i} \mathbf{A}_{ij}\mathbf{p}_j) \quad (5)$$

Here $\mathbf{p}_i$ represent the point dipoles, located at positions $\mathbf{r}_i$ and with magnitudes governed by the isotropic particle polarizabilities α_i. The total electric field $\mathbf{E}_i$ consists of the incident field $\mathbf{E}_{\mathrm{inc},i} = \mathbf{E}_0 \exp(i\boldsymbol{k}\mathbf{r}_i - i\omega t)$ and the retarded induced fields from all the other dipoles j. $\mathbf{A}_{ij}$ is a 3×3 matrix (for $i \neq j$)

$$\mathbf{A}(\mathbf{r}_{ij}) = \frac{\exp(ikr_{ij})}{r_{ij}}\left[k^2(\hat{\mathbf{n}}_{ij}\hat{\mathbf{n}}_{ij} - \mathbf{1}_3) + \frac{ikr_{ij} - 1}{r_{ij}^2}(3\hat{\mathbf{n}}_{ij}\hat{\mathbf{n}}_{ij} - \mathbf{1}_3)\right] \quad (6)$$

where $r_{ij} = |\mathbf{r}_{ij}|$, $\mathbf{r}_{ij} = \mathbf{r}_i - \mathbf{r}_j$, $\hat{\mathbf{n}}_{ij} = \mathbf{r}_{ij}/r_{ij}$, and $\mathbf{1}_3$ is the 3×3 identity matrix. By defining $\mathbf{A}_{ii} \equiv \alpha_i^{-1}$, the scattering problem reduces to a system of $3N$ complex linear equations

$$\sum_{j=1}^{N_p} \mathbf{A}_{ij}\mathbf{p}_j = \mathbf{E}_{\mathrm{inc},i} \quad (7)$$

where N_p is the total number of dipoles in the system.

A dipole polarizability is assigned to each spherical nanoparticle according to the so-called modified long-wavelength approximation (MLWA)[51]

$$\alpha = \frac{\alpha_0}{1 - \frac{2}{3}ik^3\alpha_0 - \frac{k^2}{R}\alpha_0} \quad (8)$$

$$\alpha_0 = R^3\frac{\varepsilon - n^2}{\varepsilon + 2n^2} \quad (9)$$

Here R is the radius of the sphere, which is composed of a material with frequency dependent dielectric constant ε, and α_0 is the quasi-static Clausius−Mossotti polarizability. The use of eq 8 rather than eq 9 in the CDA calculation partly compensates for finite size effects included in the full dipolar Mie expansion coefficients.

In the case of two interacting particles, $N_\mathrm{p} = 2$, the solution of eq 7 is simply

$$\mathbf{p}_1 = \frac{\alpha_1(\mathbf{E}_{\mathrm{inc},1} - \alpha_2\mathbf{A}_{12}\mathbf{E}_{\mathrm{inc},2})}{1 - \alpha_1\alpha_2\mathbf{A}_{12}\mathbf{A}_{21}} \tag{10}$$

with an analogous expression for $\mathbf{p}_2$.

With the dipole moments on the two interacting particles at hand, we can calculate the total electric field anywhere in space according to

$$\mathbf{E}(\mathbf{r}) = \mathbf{E}_{\mathrm{inc}}(\mathbf{r}) + \mathbf{A}(\mathbf{r} - \mathbf{r}_1)\mathbf{p}_1 + \mathbf{A}(\mathbf{r} - \mathbf{r}_2)\mathbf{p}_2 \tag{11}$$

The first term on the right represents the incident field, while the second and third terms are the fields from the induced dipoles on particle 1 and 2, respectively. We note that all three terms have to be included in a MST calculation, even if only the interparticle interaction is of interest.[52] The magnetic fields needed to evaluate the stress tensor are found from the Maxwell equation $\mathbf{B} = (c/i\omega)\nabla \times \mathbf{E}$, by evaluating the curl of eq 11. Thus, using the MST method, the total optical force on a single particle can be obtained by numerically integrating over a virtual sphere enclosing that particular particle. With $\mathbf{E}$ and $\mathbf{H}$ being the total electric and magnetic fields in spherical coordinates, respectively, the full expression reads[48]

$$\langle \mathbf{F}_i \rangle = \frac{1}{8\pi}\mathrm{Re}\int_0^{2\pi}\int_0^{\pi}\left\{\frac{1}{2}[n^2(E_rE_r^* - E_\theta E_\theta^* - E_\phi E_\phi^*) + (H_rH_r^* - H_\theta H_\theta^* - H_\phi H_\phi^*)]\hat{r} + (n^2E_rE_\theta^* + H_rH_\theta^*)\hat{\theta} + (n^2E_rE_\phi^* + H_rH_\phi^*)\hat{\phi}\right\} r^2 \sin(\theta)\, \mathrm{d}\theta\, \mathrm{d}\phi \tag{12}$$

2.3. Lorentz Force in the CDA (LF-CDA) and the Discrete Dipole Approximation (LF-DDA). The MST-CDA method is a "brute force" method that is comparatively costly due to the numerical integrations involved. A much more effective way of utilizing the dipole moments obtained from CDA is to directly use the Lorentz force. As we shall see in the results section, the two methods yield identical results. However, we point out that the LF-CDA method has to be implemented with care so as not to yield erroneous results.

The Lorentz force on a dipole $\mathbf{p}_i$ in an electromagnetic field is[33,52–55]

$$\mathbf{F}_i = Re(\mathbf{p}_i \cdot \nabla_i)Re(\mathbf{E}_i) + \frac{1}{c}Re\left(\frac{d\mathbf{p}_i}{dt}\right) \times Re(\mathbf{B}_i) \tag{13}$$

where $\mathbf{E}_i$ and $\mathbf{B}_i$ are the total electric and magnetic fields, respectively, c is the speed of light in vacuum and t denotes time. The incident field at the location of dipole i is specified as a plane wave, with $\mathbf{E}_{\mathrm{inc},i} = \mathbf{E}_{\mathrm{inc},0}\exp(i\mathbf{k}\cdot\mathbf{r}_i)$. For harmonic fields, time averaging of eq 13 results in

$$\langle \mathbf{F}_i \rangle = \frac{1}{2}Re[(\mathbf{p}_i^* \cdot \nabla_i)\mathbf{E}_i + ik\mathbf{p}_i^* \times \mathbf{B}_i] \tag{14}$$

where the asterisk denotes complex conjugation and $k = |\mathbf{k}|$ is the magnitude of the wave vector. Following refs 54 and 55, the time-averaged force can be split into two components, one due to the incident field and the other due to the interaction between the different dipoles, i.e. due to the induced dipole fields

$$\langle \mathbf{F}_i \rangle = \langle \mathbf{F}_{\mathrm{inc},i} \rangle + \langle \mathbf{F}_{\mathrm{int},i} \rangle \tag{15}$$

Hoekstra et al.[55] derive the following useful expressions for the two components

$$\langle \mathbf{F}_{\mathrm{inc},i} \rangle = \frac{1}{2}Re[i\mathbf{k}(\mathbf{p}_i^* \cdot \mathbf{E}_{\mathrm{inc},0})\exp(i\mathbf{k}\cdot\mathbf{r}_i)] \tag{16}$$

$$\langle \mathbf{F}_{\mathrm{int},i} \rangle = \sum_{j \neq i} \frac{1}{2}Re(\mathbf{F}_{ij}) \tag{17}$$

The interaction component is in turn determined by pairwise forces according to

$$\mathbf{F}_{ij} = \exp(ikr_{ij})\{[(\mathbf{p}_i^* \cdot \mathbf{p}_j)\hat{\mathbf{n}}_{ij} + \mathbf{p}_i^*(\hat{\mathbf{n}}_{ij} \cdot \mathbf{p}_j) + (\mathbf{p}_i^* \cdot \hat{\mathbf{n}}_{ij})\mathbf{p}_j - 5(\mathbf{p}_i^* \cdot \hat{\mathbf{n}}_{ij})\hat{\mathbf{n}}_{ij}(\hat{\mathbf{n}}_{ij} \cdot \mathbf{p}_j)]\left(-\frac{k^2}{r_{ij}^2} - \frac{3ik}{r_{ij}^3} + \frac{3}{r_{ij}^4}\right) + [(\mathbf{p}_i^* \cdot \mathbf{p}_j)\hat{\mathbf{n}}_{ij} - (\mathbf{p}_i^* \cdot \hat{\mathbf{n}}_{ij})\hat{\mathbf{n}}_{ij}(\hat{\mathbf{n}}_{ij} \cdot \mathbf{p}_j)]\left(\frac{ik^3}{r_{ij}} - \frac{k^2}{r_{ij}^2}\right) \tag{18}$$

Here $\mathbf{E}_{\mathrm{inc},0}$ is the amplitude of the incoming plane wave, $r_{ij} = |\mathbf{r}_{ij}|$, $\mathbf{r}_{ij} = \mathbf{r}_i - \mathbf{r}_j$, and $\hat{\mathbf{n}}_{ij} = \mathbf{r}_{ij}/r_{ij}$.

It is straightforward to use eqs 15−18 to obtain the force between coupled point dipoles, with moments given by eq 10. This then constitute the LF-CDA method. However, the same formalism can be used in a discrete dipole approximation (DDA) approach, which is based on a division of the interacting particles into discrete mesh elements. We use a free version of the DDA code developed by Draine and co-workers[49,50,56] together with the force calculation methodology developed by Hoekstra et al.[55] Briefly, using the DDA code, we solve for the dipole moments that build up the two particles in the dimer. Then, using eqs 15−18, we find the total force on each dipolar mesh element in both particles. The total averaged radiation forces due to all mesh elements on each particle are then obtained by summing up all elementary force contributions comprising different particles.[33–35]

In both the LF-CDA and LF-DDA methods, it is important to stress that the gradients in eq 14 refer to a given field configuration with constant dipole moments. In other words, these spatial derivatives do not include contributions that results from changes in dipole moments occurring as the result of a displacement of a particle.[55] In the case of two interacting particles, this means that the first derivative of the total field on particle 1, $\mathbf{E}_1 = \mathbf{E}_{\mathrm{inc},1} + \mathbf{A}(\mathbf{r}_{12})\mathbf{p}_2$, has to be calculated as

$$\partial\mathbf{E}_1 = \partial\mathbf{E}_{\mathrm{inc},1} + \partial[\mathbf{A}(\mathbf{r}_{12})\mathbf{p}_2] = \partial\mathbf{E}_{\mathrm{inc},1} + [\partial\mathbf{A}(\mathbf{r}_{12})]\mathbf{p}_2 \tag{19}$$

with $\mathbf{A}(\mathrm{r}_{12})$ from eq 6. In a recent publication based on LF calculations,[46] Käll and co-workers mistakenly included force contributions resulting from changing dipole moments. This lead to the erroneous result that the optical interaction force between two identical spheres, illuminated in the parallel polarization configuration, vanished under certain circumstances, thus leading to an equilibrium distance between the two particles. As we shall see in the results section, it turns out that an equilibrium separation for a homodimer only can occur for the end-fire illumination configuration. However, equilibrium separations

between dissimilar particles are in principle possible for both the parallel and perpendicular polarization configurations.

2.4. Potential Energy and Gradient Force Calculations. Gradient force and optical potential calculations probably constitute two most popular and well-known methods for estimating optical forces in the small particle limit. However, as we shall see in the results section, both methods can lead to serious errors if applied to plasmonic systems.

The potential energy experienced by a dipole i can be calculated as[57–59]

$$U_i = -\frac{1}{2}\langle \mathbf{p}_i \cdot \mathbf{E}_i^* \rangle = -\frac{1}{2}\langle \alpha_i \mathbf{E}_i \cdot \mathbf{E}_i^* \rangle = -\frac{1}{4} Re(\alpha_i)|\mathbf{E}_i|^2 \tag{20}$$

Here $\mathbf{E}_i = \mathbf{E}_{\mathrm{inc},i} + \mathbf{A}(\mathbf{r}_{ij})\mathbf{p}_j$ again represents the total electric field on dipole i, including contribution from all other dipoles as obtained from a CDA or DDA calculation. The optical force on dipole i can then be calculated as a gradient of the potential energy (20),

$$\mathbf{F}_U = -\nabla U_i = \frac{1}{4} Re(\mathbf{E}_i^* \cdot \nabla \mathbf{p}_i + \mathbf{p}_i \cdot \nabla \mathbf{E}_i^*) = \frac{1}{4} Re(\mathbf{E}_i^* \cdot \nabla \mathbf{p}_i) + \frac{1}{4}\mathrm{Re}(\alpha_i)\nabla|\mathbf{E}_i|^2 \tag{21}$$

The last term in eq 21 corresponds to the gradient force $\mathbf{F}_{\mathrm{grad}}$. However, the first term should be set to zero because it involves spatial derivatives of the dipole moments

An alternative way of introducing a potential energy would be through a line integral of the total optical force

$$U_F = -\int_{\infty}^{r_0} \mathbf{F}\, \mathrm{d}\mathbf{r} \tag{22}$$

or as the integral of the gradient force (if the nongradient force contribution is small)

$$U_{\mathrm{grad}} = -\int_{\infty}^{r_0} \mathbf{F}_{\mathrm{grad}}\, \mathrm{d}\mathbf{r} \tag{23}$$

Provided that the force only depends on the position of the particle and the motion is restricted to one dimension, this yields an unambiguous definition of a potential, even though the total optical force, i.e. including scattering contributions, is not conservative.

3. Results and Discussion

We analyze optical forces between two metal nanospheres illuminated in three different polarization configurations, as shown in Figure 1. The surrounding medium is water ($n = 1.33$) and the dielectric constants of the particles correspond to silver or gold.[60] The intensity of the incident plane wave is set to 1 W/μm^2. In the following, we will display results for both a symmetric case, i.e., both particles have the same radii ($R_1 = R_2 = 5$ nm), and asymmetric cases for which particle 1 has radius $R_1 = 10$ nm and particle 2 has a radius in the range $R_2 = 20-40$ nm.

3.1. Optical Forces between Identical Nanospheres. We begin by analyzing the force acting on one of the particles in a homodimer composed of two 5 nm radius Au spheres. Figure 2 shows the optical interparticle force versus photon energy for

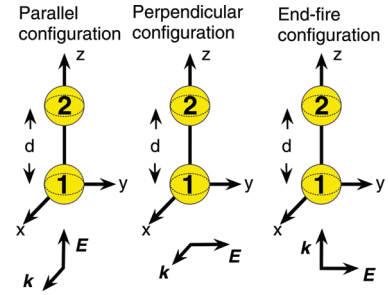

Figure 1. Illumination configurations for the two-particle (dimer) system in the presence of a plane wave. The wave-vector of the incident wave is denoted by $\boldsymbol{k}$ and its polarization by $\boldsymbol{E}$.

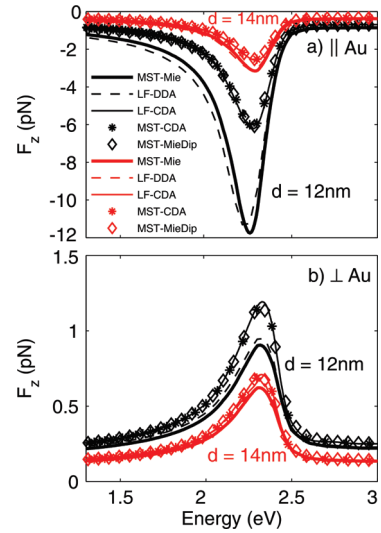

Figure 2. Spectra of the optical force between two gold spheres with radii $R_1 = R_2 = 5$ nm for an intensity of the incident field of 1 W/μm^2. The center-to-center separation distances between the nanoparticles are $d = 12$ nm (black lines) and $d = 14$ nm (red lines). The polarization of the incident field is either parallel (a) or perpendicular (b) to the dimer axis. The optical forces are calculated using the following methods: MST-Mie ($l_{max} = 13$, thick solid lines); LF-DDA (dashed lines); LF-CDA (thin solid lines); MST-CDA (stars); and MST-MieDip ($l_{\max} = 1$, diamonds).

the parallel (Figure 2a) and the perpendicular (Figure 2b) polarization configurations. Referring to Figure 1, we display the z component of the force on particle 2; that is, a positive value means that the force between the particles is repulsive, and vice versa. We use three different calculation methods in the dipole limit (LF-CDA, MST-CDA and MST-MieDip) and two methods (MST-Mie and LF-DDA) that include higher multipole responses. Results are displayed for two different interparticle distances, $d = 12$ and 14 nm, corresponding to surface-to-surface separations of 2 and 4 nm, respectively.

All curves in Figure 2 are dominated by the strong dipolar plasmon resonance at ~2.3 eV. The force is attractive for the parallel configuration and repulsive for the perpendicular configuration. This difference can be understood from the distribution of induced charges, as discussed in the following paragraph. For parallel polarization, the magnitude of the force increases strongly with decreasing distance d between particles. This is a direct consequence of the increasing field-enhancement between the particles.[30] At the same time, the spectral position of the force maximum red-shifts due to plasmon hybridization. For the perpendicular configuration, on the other hand, the coupling between the elementary dipoles leads to a slight blue shift of the force maximum with decreasing d.

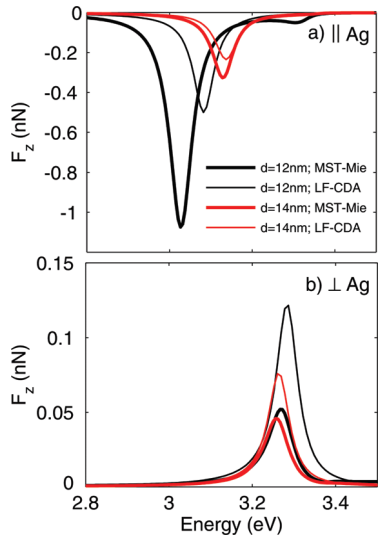

Figure 3. Same plots as in Figure 2, but for the case of two 5 nm silver particles and only including MST-Mie ($l_{max} = 13$) and LF-CDA calculations.

Regarding the differences between the various calculation methods, we first note that the calculations based on the dipole approximation all fall on the same curve. However, there is a clear difference between the dipole approximation calculations, on the one hand, and the MST-Mie (here with $l_{max} = 13$) and LF-DDA calculations, on the other. This difference becomes more pronounced for smaller interparticle separations because electrostatic contributions to the induced fields that are neglected in the dipole limit then become more pronounced. These contributions are taken into account by including a large number of multipoles in the MST-Mie calculation and by using a small enough mesh size in the LF-DDA method. In particular, the dipole calculations underestimate the field-enhancement, and thereby the attractive force, in the gap between the particles for the parallel polarization configuration. For the perpendicular polarization, on the other hand, the dipole models overestimate the repulsive force between the particles. This is a result of neglecting attractive multipole couplings in the dipole limit, for example dipole-quadropole interactions. We shall also point out that there is a small but clear difference between the MST-Mie and LF-DDA calculations. In the present case, we use a mesh size of 0.20 nm (about 130 000 mesh elements), which is not enough to completely represent all relevant multipoles in a case where the interparticle separation is comparable with the mesh size. In order to get improved agreement with the MST-Mie theory, we would have to increase the number of mesh elements, and thus the calculation time, beyond what is feasible. It is then clear that the MST-Mie theory is both the most exact and the fastest method for calculating the interparticle forces we are considering here, i.e. between spherical particles. Regarding the dipole methods used, we have previously mentioned that MST-CDA is the least useful, because it is much more time-consuming compared to LF-CDA and MST-MieDip. In the following, we will therefore only use LF-CDA for calculations in the dipole limit, while the full MST-Mie method is used to obtain exact results.

To further illustrate the difference between the dipole limit and full Mie theory, Figure 3 shows the same type of results as Figure 2 but for the case of silver particles. From a qualitative point of view, the results are similar to the ones found for gold. Notice, however, that the magnitude of the force now is measured in nN rather than pN. This is of course a result of the dielectric properties of silver, which is more polarizable than gold and also exhibits a considerably smaller optical damping in the frequency range of interest. This leads to higher dipole moments on the particles, which in turn are further enhanced by the particle−particle interaction. A further consequence of this is that the discrepancy between the results from the LF-CDA and MST-Mie methods becomes more distinct. The importance of higher multipoles is obvious from Figure 3a, where for $d = 12$ nm, the optical force exhibits a higher-order mode around 3.3 eV.

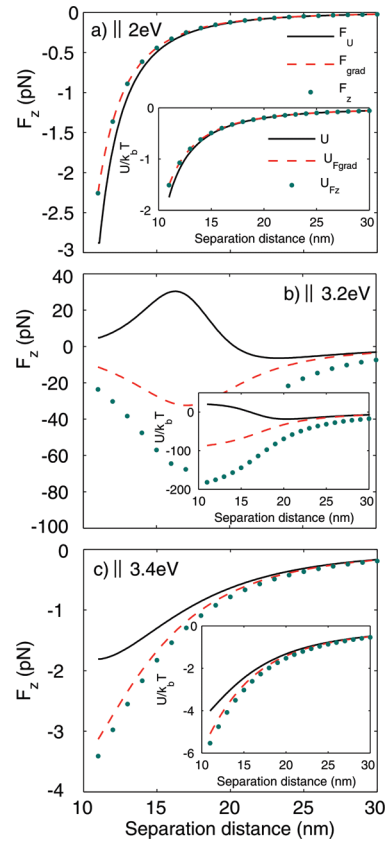

Figure 4. Optical forces between two silver nanoparticles ($R_1 = R_2 =$ 5 nm) as a function of the center-to-center separation distance for different photon energies. The polarization is parallel to the dimer axis. F_z and U_{Fz} denote the interparticle force and potential, respectively, in the point dipole limit (CDA-LF method). F_U and U are calculated from the classical expression for the potential energy of a dipole in an applied field. F_{grad} and U_{Fgrad} correspond to gradient force calculations. The potentials are normalized to the thermal energy k_BT, with $T = 300$ K.

Figure 4 shows optical forces versus separation for two silver particles illuminated in the parallel configuration at three different photon energies. The "correct" optical force in the dipole limit, F_z, is calculated using the LF-CDA method. This is compared to the gradient force F_{grad} obtained from the last term in eq 21 and F_U, which is calculated as a spatial derivative of the classical expression for the potential energy of a dipole in an applied field, i.e., eq 20. The latter energy is shown as an inset and denoted U, but we also show the potential energies that correspond to F_z and F_{grad}, which are obtained as integrals according to eq 22 and 23, respectively.

Figure 4a shows an out-of resonance case ($\hbar\omega = 2$ eV), where the optical force between the two particles is rather weak. The agreement between the "correct" force F_z and the gradient force F_{grad} is then more or less perfect, as is the case for the potentials U_{Fz} and U_{grad} in the inset. The small deviations compared to the potential U and the optical force F_U for small separation

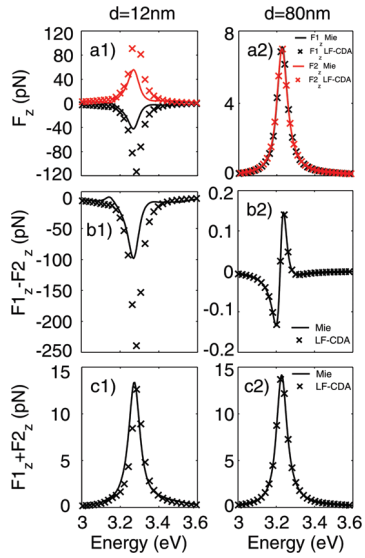

Figure 5. Spectra of the optical forces between two equal silver nanoparticles ($R_1 = R_2 = 5$ nm) in the case of an end-fire illumination configuration. The intensity of the incident light is 1 W/μm^2. The center-to-center separation distances are $d = 12$ nm (left column: (a1−c1)) and $d = 80$ nm (right column: (a2−c2)). The optical forces are calculated using the Mie-MST ($l_{max} = 13$) method (solid lines) and the LF-CDA method (crosses). The first row (a1−a2) shows the total optical forces in the z direction on each particle (black curves represents forces on particle 1 and red color represents forces on particle 2). The second and third rows show the binding (b1−b2) and the total (c1−c2) forces between both particles, respectively.

distances occur because of the derivatives of the dipole moments that are hidden in eq 20.

Figure 4b highlights two interesting effects that occur for illumination with photons close to resonance ($\hbar\omega = 3.2$ eV). The first is the rather large deviations of U and F_U from the correct values of the potential, U_{Fz}, and the optical force F_z. Moreover, the potential energy shows an equilibrium position between the two particles, something that is obviously not correct. The second effect is a deviation of the gradient force F_{grad} from the total force F_z. Since the imaginary part of the polarizability is rather large at or near resonance, it is no longer correct to identify the optical force with just the gradient force. Notice also that, as a result of the resonance, the optical force is much stronger than in Figure 4a.

In Figure 4c the photon energy is increased to $\hbar\omega = 3.4$ eV, which corresponds to a negative value of the real part of the polarizability. Still the optical force between the particles is attractive also in this case. A negative value of the polarizability means only that dipole moments induced in the particles are oriented opposite to the incident field. But since both particles are still polarized in the same way relative to each other, the force between them is also now attractive. This is further discussed and explained in more detail when we deal with the case of differently sized particles.

The results in Figure 4 show that one should be careful when using the potential energy or the gradient force in the dipole approximation. This is especially true near resonance and in case of materials with small damping, such as silver.

Although the equilibrium distance seen for a homodimer in Figure 4b turned out to be an artifact, illumination in the end-fire geometry actually can lead to a vanishing interparticle force. Figure 5 shows the optical forces on each of the two silver particles in the z direction (a1−a2), together with binding (b1−b2), and total forces (c1−c2), for the end-fire configuration. A positive value means that the corresponding force is directed in the positive z direction. The total force is always positive and does not change much when the particle separation changes. This means that the two particles, by the influence of the light pressure, float together in the direction of the incident $\boldsymbol{k}$ wave vector, i.e., in the positive z direction. However, as we see from Figure 5b, the binding force can be zero. Physically, this means that two particles float together in the z direction with a constant relative distance between them.

When the distance between particles is large ($d = 80$ nm), the MST-Mie and LF-CDA methods, as expected, agree perfectly. For smaller separation distances, the LF-CDA method does not predict an equilibrium position. While for large separation distances the equilibrium distance is a result of retardation effects, for small separations the optical force becomes zero because of higher-mode interactions. Note that the forces on particles 1 and 2 (Figure 5a1-a2) point toward each other for $d = 12$ nm, while for $d = 80$ nm they are both directed in the positive z direction. To summarize, for small separation distances, the main contribution to the total force comes from the interaction between dipoles $F_z \approx F_{int}$ (eq 17) resulting in an attractive force, whereas for large separation distances the total force $F_z \approx F_{inc}$ (eq 16) points in the direction of the incident $\boldsymbol{k}$ wave vector, while also retardation effects become important.

3.2. Optical Forces between Nonidentical Nanospheres. We now turn to the more realistic case of heterodimers. To clearly illustrate the effect of symmetry breaking, we need to avoid broadening due to interband transitions. We therefore first use a Drude function, with plasma frequency $\omega_p = 8$ eV and damping $\Gamma = 0.1$ eV, to describe the dielectric response of the particles. Referring to Figure 1, we study a case in which particle 1 has a fixed radius of $R_1 = 10$ nm while the radius of particle 2 varies between 10 and 40 nm. Figure 6 (a1 and b1) shows the optical force on particle 1 in the z direction, with positive values corresponding to attraction, for the parallel and perpendicular illumination configurations, respectively.

For the homodimer ($R_1 = R_2 = 10$ nm) in the parallel (perpendicular) polarization configuration, the force is attractive (repulsive) just as for the 5 nm radii spheres studied in the preceding section. However, by increasing the radius of particle 2, we see that the optical force now can change sign as a function of photon energy for both polarization configurations. Specifically, in the case of parallel polarization we see a new repulsive (negative) peak develop at high energies when the radius of particle 2 increases. Similarly, for perpendicular polarization, we see a new attractive (positive) peak develop at energies lower than the original hybridized dipole resonance of the homodimer. Both peaks are also seen in extinction spectra, shown in Figure 6 (a3 and b3) for completeness, but the relative amplitudes are very different compared to the force spectra. This is because the latter are dominated by optical near-fields, while only far-fields contribute to the extinction spectra.

The behavior of the optical force can be qualitatively interpreted and explained by considering the phase differences between the dipoles excited on particle 1 and 2, see Figure 6 (a2 and b2). For both polarization configurations, the dipoles oscillate out of phase whenever the phase difference is greater than $\pi/2$. This means that the charge interactions revert compared to the homodimer case, one obtains a repulsive force for the parallel case and an attractive force for perpendicular polarization. The reason why we at all can see a substantial phase difference between the two particles is of course that the resonance positions change with size. Specifically, an increasing radius leads to a red shift, which implies that the hybridized

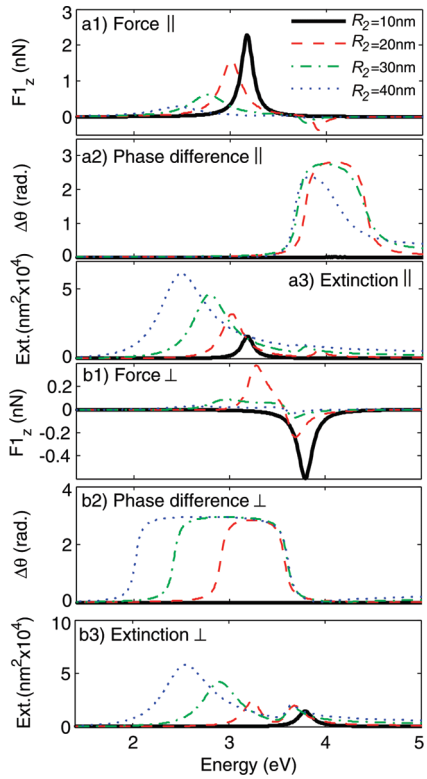

Figure 6. Spectra of the optical interparticle force calculated using the CDA-LF method and a Drude dielectric function for parallel (a1) and perpendicular (b1) polarization configurations, respectively. Particle 1 has radius $R_1 = 10$ nm, particle 2 varies between $R_2 = 10-40$ nm, and the edge-to-edge distance is fixed to $d_{edge} = 2$ nm. Figures (a2) and (b2) show the phase differences $\Delta\theta = \theta_1 - \theta_2$ between the dipole moments induced in particles 1 and 2. Extinction spectra of the dimers calculated with the CDA method are shown in (a3) and (b3) for parallel and perpendicular polarizations, respectively.

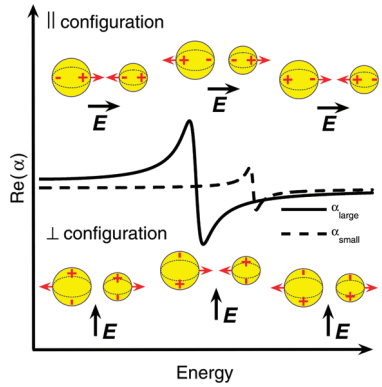

Figure 7. Schematic illustration of induced dipole charges in a heterodimer illuminated with polarization parallel (upper row) and perpendicular (lower row) to the dimer axis. The curves illustrate the real parts of the polarizabilities for the large and the small particle versus energy.

peak at low energy and parallel polarization is dominated by the large particle in the pair, while the small peak at high energy is dominated by the 10 nm particle. To further illustrate this effect, we show in Figure 7a schematic illustration of how the resonance positions, shown through the real part of the dipole polarizabilities, dictate the interparticle force for a heterodimer. Three different energy ranges can be distinguished, i.e., corresponding to photon energies below, between and above the two resonance energies. As can be seen in the figure, for parallel polarization, opposite charges face each other in the low- and

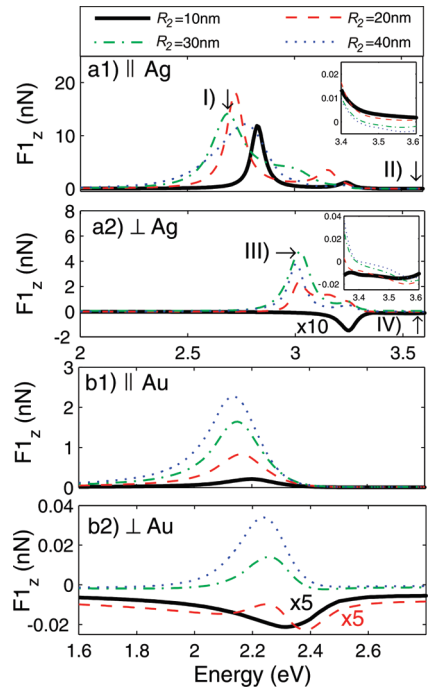

Figure 8. Force spectra for heterodimers ($R_1 = 10$ nm, $R_2 = 10$ - 40 nm, $d_{edge} = 2$ nm) composed of Ag and Au spheres calculated with the MST-Mie ($l_{max} = 30$) method in the parallel (a1−a2) and perpendicular (b1−b2) polarization configuration. The arrows mark energies for field plots in Figure 9.

high-energy regions, leading to attraction, even though the polarizabilities have different signs in the two energy ranges, and repulsion can only occur in the intermediate energy range. The same argument explains why attraction can occur in the intermediate energy region for perpendicular polarization.

The behavior of the coupled system of particles in Figure 6 is of course much more complex than what is illustrated in Figure 7, where we have assumed that the resonances refer to single isolated particles. In particular, Figure 7 can be misleading in cases when one of the particles in the heterodimer is much larger than the other one. If this is the case, the scattered field from the large particle (particle 2 in Figure 6) becomes so large compared to the incident field that it forces the dipole on the small particle to oscillate in phase. Accordingly, with increasing radius of particle 2, the optical force between the particles becomes attractive over a much broader energy range, irrespective of polarization configuration. This is clearly seen for the $R_2 = 40$ nm case in Figure 6. Nevertheless, the overall picture sketched in Figure 7 still seems to be valid, but the question is how much it is affected by introducing multipoles and the actual metal dielectric functions of Ag and Au.

Figure 8 shows force calculations for the same particle sizes as in Figure 6, but with silver (a1−a2) and gold (b1−b2) dielectric functions and using the MST-Mie ($l_{max} = 30$) theory. A comparison with Figure 6 reveals rather drastic differences, in particular at higher photon energies, where multipolar effects becomes dominant in the case of Ag and interband damping sets in for the Au case. In particular, for the Ag dimer and parallel polarization case, we see a strong suppression of the "repulsive region", evident for $R_2 = 30-40$ nm in Figure 6 (a1). It is only at very high energies (inset in Figure 8 a1), indicated by the arrow marked II, for which a weak repulsive interaction remains. In Figure 9, we show the corresponding field distributions in the gap region, demonstrating a weak repulsion at high energies and a strong attraction near the main

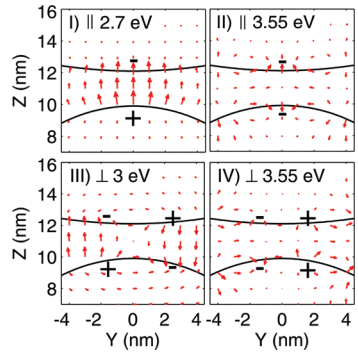

Figure 9. Electric field plots for the $R_1 = 10$ nm, $R_2 = 30$ nm Ag heterodimer for the energies marked with arrows in Figure 8. The plots show the real parts of the normalized electric field in Y and Z directions in the plane $X = 0$ from MST-Mie theory ($l_{max} = 30$). Solid black lines represent the edges of the particles.

dipole resonance (arrow marked I in Figure 8 a1). The situation is similar for the perpendicular polarization configuration and the Ag case, i.e. attractive interactions start to dominate as soon as the homodimer symmetry is broken and it is only at high energy (arrow marked IV and inset in Figure 8 a2) for which a weak repulsion remains. Turning to the case of Au dimers and parallel polarization, Figure 8 (b1), we in fact find a complete cancelation of the "repulsive region", but in this case due to strong interband damping. On the other hand, for perpendicular polarization (Figure 8 b2), one do see a rather clear transition from an attractive to a repulsive force for the heterodimers with $R_2 = 30$ and 40 nm, but the effect is not very large.

4. Summary and Conclusions

We have calculated optical interparticle forces between two small metal spheres. The calculations show that the optical force is always attractive (repulsive) for a homodimer illuminated in the parallel (perpendicular) polarization configuration. However, in the end-fire configuration and in the case of heterodimers it is in principle possible to get a transition from an attractive to a repulsive force as a function of interparticle distance, thus enabling an equilibrium distance. We show that calculations in the dipole limit are extremely useful as a tool for physical understanding. However, multipoles generally contribute attractive interactions that cannot be neglected at small interparticle separations. We have also found that the often-used dipole potential energy and gradient force equations only are valid for weakly interacting dipoles.

Acknowledgment. We thank Timur Shegai, and Lianming Tong for stimulating discussions. This work was financially supported by the Swedish Research Council.

References and Notes

(1) Moskovits, M. *J. Chem. Phys.* **1978**, *69* (9), 4159–4161.
(2) Moskovits, M. *Rev. Mod. Phys.* **1985**, *57*, 783–826.
(3) Lambe, J.; McCarthy, S. L. *Phys. Rev. Lett.* **1976**, *37*, 923.
(4) Berndt, R.; Gimzewski, J. K.; Johansson, P. *Phys. Rev. Lett.* **1991**, *67*, 3796.
(5) Fleischmann, M.; Henra, P. J.; McQuillan, A. J. *Chem. Phys. Lett.* **1974**, *26* (2), 163.
(6) Jeanmaire, D. L.; Van Duyne, R. P. *J. Electroanal. Chem.* **1977**, *84*, 1–20.
(7) Albrecht, M. G.; Creighton, J. A. *J. Am. Chem. Soc.* **1977**, *99* (15), 5215–5217.
(8) Anker, J. N.; Hall, W. P.; Lyandres, O.; Shah, N. C.; Zhao, J.; van Duyne, R. P. *Nat. Mater.* **2008**, *7*, 442.
(9) Sepúlveda, B.; Angelomé, P. C.; Lechuga, L. M.; Liz-Marzán, L. M. *Nano Today* **2009**, *4*, 244–251.
(10) Gobin, A. M.; Lee, M. H.; Halas, N. J.; James, W. D.; Drezek, R. A.; West, J. L. *Nano Lett.* **2007**, *7*, 1929.
(11) Mühlschlegel, P.; Eisler, H. J.; Martin, O. J. F.; Hecht, B.; Pohl, D. W. *Science* **2005**, *308*, 1607.
(12) Pakizeh, T.; Käll, M. *Nano Lett.* **2009**, *9*, 2343.
(13) Smith, D. R.; Pendry, J. R.; Wilthire, M. C. K. *Science* **2004**, *305*, 788.
(14) Ashkin, A.; Dziedzic, J. M.; Bjorkholm, J. E.; Chu, S. *Opt. Lett.* **1986**, *11* (5), 288–290.
(15) Prikulis, J.; Svedberg, F.; Käll, M.; Enger, J.; Ramser, K.; Goksör, M.; Hanstorp, D. *Nano Lett.* **2004**, *4* (1), 115–118.
(16) Hansen, P. M.; Bhatia, V. K.; Harrit, N.; Oddershede, L. *Nano Lett.* **2005**, *5* (10), 1937–1942.
(17) Tong, L. M.; Miljkovic, D. V.; Käll, M. *Nano Lett.* **2010**, *10*, 268–273.
(18) Novotny, L.; Bian, R. X.; Xie, X. S. *Phys. Rev. Lett.* **1997**, *79*, 645.
(19) Okamoto, K.; Kawata, S. *Phys. Rev. Lett.* **1999**, *83*, 4534 Chaumet P. C. .
(20) Rahmani, A.; Nieto-Vesperinas, M. *Phys. Rev. Lett.* **2002**, *88*, 123601.
(21) Quidant, R.; Petrov, D.; Badenes, G. *Opt. Lett.* **2005**, *30* (9), 1009–1011.
(22) Rhighini, M.; Zelenina, A. S.; Girard, C.; Quidant, R. *Nat. Phys.* **2007**, *3*, 477–480.
(23) Righini, M.; Girard, C.; Quidant, R. *J. Opt. A: Pure Appl. Opt.* **2008**, *10*, 093001.
(24) Grigorenko, A. N.; Roberts, N. W.; Dickinson, M. R.; Zhang, Y. *Nat. Photonics* **2008**, *2*, 365–370.
(25) Juan M. L.; Gordon R.; Pang Y.; Eftekhari F.; Quidant R. *Nat. Photonics* **2009**, doi: 10.1038/nphys1422.
(26) Xu, H. X.; Bjerneld, E. J.; Käll, M.; Borjesson, L. *Phys. Rev. Lett.* **1999**, *83* (21), 4357–4360.
(27) Xu, H. X.; Aizpurua, J.; Käll, M.; Apell, P. *Phys. Rev. E* **2000**, *62* (3), 4318–4324.
(28) Xu, H. X.; Wang, X. H.; Persson, M. P.; Xu, H. Q.; Käll, M.; Johansson, P. *Phys. Rev. Lett.* **2004**, *93* (24), 243002.
(29) Johansson, P.; Xu, H. X.; Käll, M. *Phys. Rev. B* **2005**, *72* (3), 035427.
(30) Xu, H. X.; Käll, M. *Phys. Rev. Lett.* **2002**, *89* (24), 246802.
(31) Chaumet, P. C.; Nieto-Vesperinas, M. *Phys. Rev. B* **2001**, *64*, 035422.
(32) Hallock, A. J.; Redmond, P. L.; Brus, L. E. *Proc. Natl. Acad. Sci. U.S.A.* **2005**, *102* (5), 1280–1284.
(33) Wong, V.; Ratner, M. A. *J. Opt. Soc. Am. B* **2006**, *23* (9).
(34) Wong, V.; Ratner, M. A. *Phys. Rev. B* **2006**, *73*, 075416.
(35) Wong, V.; Ratner, M. A. *J. Opt. Soc. Am. B* **2007**, *24* (1).
(36) Zelenina, A. S.; Quidant, R.; Nieto-Vesperinas, M. *Opt. Lett.* **2007**, *32* (9), 1156–1158.
(37) Chu, P.; Mills, D. L. *Phys. Rev. Lett.* **2007**, *99*, 127401.
(38) Chu, P.; Mills, D. L. *Phys. Rev. B* **2008**, *77*, 045416.
(39) Ng, J.; Tang, R.; Chan, C. T. *Phys. Rev. B* **2008**, *77*, 195407.
(40) Li, Z.; Käll, M.; Xu, H. X. *Phys. Rev. B* **2008**, *77*, 085412.
(41) Novotny L.; Henkel C. *Opt. Lett.* **2008**, *33* (9).
(42) Nome, R. A.; Guffey, M. J.; Scherer, N. F.; Gray, S. K. *J. Phys. Chem. A* **2009**, *113*, 4408–4415.
(43) Svedberg, F.; Li, Z. P.; Xu, H. X.; Käll, M. *Nano. Lett.* **2006**, *6* (12), 2639–2641.
(44) Svedberg, F.; Käll, M. *Faraday Disc.* **2006**, *132*, 35–44, Tong LM.
(45) Righini, M.; Gonzalez, M. U.; Quidant, R.; Käll, M. *Lab Chip* **2009**, *9* (2), 193–195.
(46) Sepulveda, B.; Alegret, J.; Käll, M. *Opt. Exp.* **2007**, *15* (22), 14914–14920.
(47) Johansson, P. Unpublished.
(48) Barton, J. P.; Alexander, D. R.; Schaub, S. A. *J. Appl. Phys.* **1989**, *66* (10).
(49) Draine, B. T. *Astrophys. J.* **1988**, *333*, 848–872.
(50) Draine, B. T.; Flatau, P. J. *J. Opt. Soc. Am. A* **1994**, *11*, 1491–1499.
(51) Meier, M.; Wokaun, A. *Opt. Lett.* **1983**, *8* (11).
(52) Novotny, L. *Top. Appl. Phys.* **2001**, *81*, 123.
(53) Gordon, J. P. *Phys. Rev. A* **1973**, *8*, 14–21.
(54) Draine, B. T.; Weingartner, J. C. *Astrophys. J.* **1996**, *470*, 551–565.
(55) Hoekstra, A. G.; Frijlink, M.; Waters, L. B. F. M.; Sloot, P. M. A. *J. Opt. Soc. Am. A* **2001**, *18* (8).
(56) Draine, B. T.; Flatau, P. J. http://arxiv.org/abs/0809.0337v4.
(57) Novotny, L.; Hecht B. *Principles of nano-optics*; Cambridge University Press: 2006.
(58) Novotny, L.; Henkel C. *Opt. Lett.* **2008**, *33* (9).
(59) Jackson, J. D. *Classical Electrodynamics*, 3rd ed.; Wiley: New York, 1998.
(60) Johnson, P. B.; Christy, R. W. *Phys. Rev. B* **1972**, *6*, 4370–4379.

JP911371R